Meteorol Atmos Phys 88, 237–250 (2005)
DOI 10.1007/s00703-004-0075-x

Meteorology and Atmospheric Physics
Printed in Austria

Department of Meteorology, The Florida State University, Tallahassee, Florida

Anomalous gradient winds in the subtropical jet stream and interpretations of forecast failures

T. N. Krishnamurti, P. Cunningham, and **K. Rajendran**

With 12 Figures

Received September 29, 2003; accepted December 8, 2003
Published online: July 8, 2004

Summary

Dramatic examples of forecast failures in global models of moderate resolution (i.e., T106) have been shown to occur during periods of the negative phase of the Pacific/North American (PNA) pattern in the Northern Hemisphere winter. Specifically, in these periods forecast skills at 500 hPa as measured by the standard anomaly correlation index dropped to rather low values by days 4 and 5 of the forecasts. This paper examines systematically some of the factors that may have contributed to the failure of these model forecasts.

In particular, strong winds approaching intensities on the order of $100\,\mathrm{m\,s^{-1}}$ south of Japan at the 200 hPa level were degraded by the initialization and data assimilation procedures of the models. These observed winds were found to be supergradient in nature and representative of the anomalous solution of the gradient wind equation. Procedures such as the multivariate optimum interpolation (with its geostrophic constraints) and the normal-mode initialization including several vertical modes apparently were factors that led to the degradation of these strong winds in the initial model states. In this paper, an analysis of these factors is presented, and it is shown that uninitialized analyses (with no constraints) based on a simple successive correction procedure can retain the strong winds evident in the observations. Forecasts thus performed appear to retain wave trains, a characteristic feature of negative PNA initial states, leading to a significant improvement in forecast skill.

1. Introduction

In this paper, we explore the importance of supergradient winds in the upper troposphere, especially near the subtropical jet stream, over Southern Japan. Over this region, wind speeds on the order of $100\,\mathrm{m\,s^{-1}}$ are often reported in upper-air observations. The corresponding pressure gradients are generally quite weak and are not consistent with wind speeds based on geostrophic or gradient wind relationships. An examination of past data sets along a chain of Japanese upper-air stations shows that, in any month of the Northern Hemisphere winter, roughly one third of the time such strong winds are indeed found at the 200 hPa level. Mogil and Holle (1972) noted the infrequent presence of such winds over the United States along the subtropical jet stream at the 200 hPa level. They referred to these winds as anomalous winds; that is, the wind speeds were more representative of the anomalous solution of the gradient wind equation (e.g., Holton, 1992, Sect. 3.2.5). Moreover, they noted that these strong winds were generally slightly stronger than twice the geostrophic wind.

Palmer (1988) examined several examples of global model forecasts in which the forecast skills measured by the anomaly correlation index were quite low. This decrease in skill was observed after days 4 and 5 of the forecasts. Furthermore, Palmer (1988) noted that these low skills were often seen in the Northern

Hemisphere winter season during the negative phase of the Pacific/North American (PNA) teleconnection pattern. Negative PNA indices are generally characterized by a positive 500 hPa geopotential height anomaly over the Aleutian Islands and negative 500 hPa geopotential height anomalies over the tropical Pacific and the Rockies. During these events a characteristic negative PNA wave train has also been identified from observational data sets. The phase of this wave train is generally the inverse of the well-known PNA wave train (Wallace and Gutzler, 1981).

The inability of global forecast models either to predict or to maintain the negative PNA wave train was considered to be an important factor for these forecast failures. In this regard, Palmer (1988) alluded to the possible need for the models to resolve barotropic instability, highlighting a dynamical deficiency of the then-current models. Palmer also clearly showed a strong negative correlation between the forecast skill and the PNA index based on 18 such forecasts. The resolutions of global spectral models in the 1980s were at best described by 106 waves (triangular truncation). Resolving barotropic instability often requires higher resolution and better initial data coverage than was available at that time. Although model resolutions have improved over the recent decades, the data coverage has remained somewhat unchanged. High-level cloud tracked winds seen from the Japanese geostationary satellite (GMS) have been available during the entire period of the 1980s. Commercial aircraft wind reports near the 200 hPa level have also shown a similar data coverage south of Japan during this period.

In diagnosing the data sets for several of the forecast failures reported by Palmer (1988), we have found that anomalous supergradient winds were frequently present in the new data sets but were not contained in the initial states of the global forecast models. In this paper, we examine some of these same examples to provide further insight into these forecast failures. Specifically, we demonstrate a link between the forecast failures and the occurrence of anomalous supergradient winds in the upper troposphere. This analysis explores observational evidence for the presence of such winds, and some specific model deficiencies that existed and may have contributed to an overbalancing of the wind field in relation to the pressure field. Furthermore, we show that by retaining these supergradient winds in the model's initial state, some of those forecast failures may be avoided.

In the following section, we provide a brief review of anomalous gradient winds and present evidence for their existence in the subtropical jet near Japan. The possible role of initialization and data assimilation procedures in removing these winds is discussed in Sect. 3, while in Sect. 4 we present several numerical experiments with a global forecast model that assess the impact on forecast skill of the inclusion of these winds in the initial state. Finally, in Sect. 5 we discuss the major conclusions arising from this paper, their implications for numerical weather prediction in general, and suggest possible directions for future research.

2. Supergradient winds south of Japan

At 200 hPa during the Northern Hemisphere winter season, the subtropical jet achieves maximum wind speeds on the order of $100\,\mathrm{m\,s^{-1}}$ on many days during each month. A chain of upper-air weather stations lies along the length of Japan from south to north. We can regard this chain of stations as an irregularly spaced grid where direct wind and geopotential height observations are available twice a day at 00 UTC and 12 UTC. Thus, in principle, we can calculate the gradient wind departures of the observed winds along this line.

We shall first provide a brief review of the dynamics of the supergradient wind (see also Holton, 1992, Sect. 3.2). In the natural coordinate system, an expression of force balances normal to the direction of the flow results in the expression

$$K_T V_G^2 + f\,V_G = f\,V_g, \tag{1}$$

where $K_T = 1/R_T$, with R_T the radius of trajectory curvature, V_G is the gradient wind, V_g is the geostrophic wind, and f is the Coriolis parameter.

Solving the above equation for $1/V_G$ and inverting, we obtain two solutions for the gradient wind:

$$V_N = \frac{2V_g}{1 + (1 + 4K_T V_g/f)^{1/2}}, \tag{2}$$

and

$$V_A = \frac{2V_g}{1-(1+(4K_T V_g/f))^{1/2}}. \quad (3)$$

Equation (2) is the solution for the "normal" gradient wind, whereas (3) describes the so-called "anomalous" gradient wind. A zero radical produces the following relationship as a lower limit for the anomalous solution:

$$V_G = 2V_g \quad (4)$$

so that for anomalous gradient wind balance, the wind speed must be greater than or equal to twice the geostrophic wind speed. This is an important limit for these flows.

Figure 1 illustrates the two solutions for the gradient wind equation (1) during an anticyclonic flow. Here, the dashed curve represents the inertial wind (i.e., $-fR_T$) when the geostrophic wind (V_g) becomes zero. The normal gradient wind solution (2) is valid for the region with $V_G \leq 2V_g$. The normal solution reduces to geostrophic flow as the radius of trajectory curvature becomes very large. The anomalous gradient wind solution (3) is valid for the region where $V_G > 2V_g$. The upper bound of the anomalous solution has been shown to be that of the inertial wind when the geostrophic wind approaches zero (Newton, 1959).

Next, we shall illustrate the presence of these features in the Japan data sets. Only days on which the intensity of the wind at 200 hPa was greater than 100 kts are considered here. In order to assess whether the observed winds were supergradient, the geostrophic wind was first computed, assuming that all the height values are on the same axis. This is aided by the climatological data (Fig. 2). Using the fact that **n** is to the left and perpendicular to the flow (the flow is zonal), $\partial\phi/\partial n$ can be computed using finite differences (i.e., in the direction of **n**).

In Table 1, we show a sample of the evidence for supergradient winds for several days when strong winds were encountered at 200 hPa along the Japan network of upper-air stations. These upper-air stations are roughly located from south to north along the mean longitude of Japan. The first column identifies the date (month, day, and year). The second column identifies the latitude of the upper-air station; longitudes are not relevant since we are looking at the gradient winds along roughly 140° E. The next two columns respectively identify the wind direction and speed ($m\,s^{-1}$). The

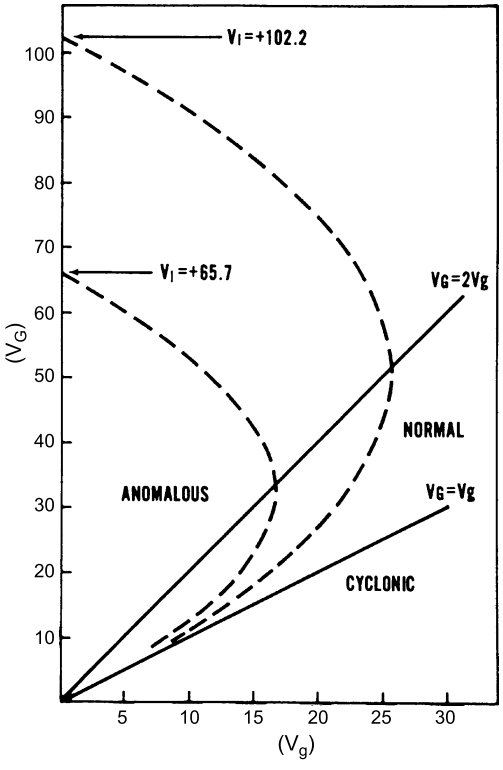

Fig. 1. Plot of geostrophic, V_g, versus gradient, V_G, winds ($m\,s^{-1}$) showing the double solution for the gradient wind equation during anticyclonic flow. Dashed curves represent two values of ($-fR_T$) which becomes the inertial wind when $V_g = 0$

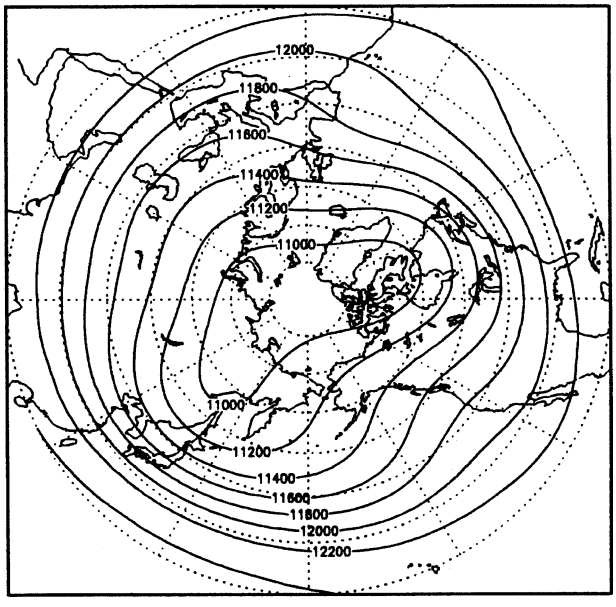

Fig. 2. Mean 200 hPa geopotential height in the Northern Hemisphere for the period 1979 to 1995

Table 1. Observed supergradient winds for stations in southern Japan for the period 1960–1963

Date (mmddyy)	Latitude (°N)	Direction (°)	Speed (m/s)	Height (m)	V/Vg
010160	31.52	240	69.50	11990	5.551187
010160	33.20	240	54.35	12130	1.152106
010160	37.23	250	72.51	11870	1.171442
010260	31.52	250	69.61	11870	2.780026
010260	37.23	260	68.90	11450	1.001790
010260	38.18	260	43.50	11560	1.606484
010260	43.13	260	44.95	11300	1.101596
010660	31.52	260	94.73	11830	1.081000
010660	33.20	260	92.71	11900	1.746835
011060	33.20	270	81.79	11950	1.155867
011160	33.20	260	83.08	11820	1.280839
011860	33.20	280	81.56	11810	1.063962
012560	33.20	260	98.28	11850	1.041658
012560	39.40	270	50.92	11360	1.174637
012960	31.52	260	94.73	11800	1.081000
012960	33.20	260	89.67	11870	1.086147
013160	33.20	250	92.81	11850	5.246356
010761	31.52	260	105.37	12020	1.489106
011161	31.52	250	85.56	11960	1.139039
011561	43.13	260	81.69	11330	1.087557
011561	31.52	250	50.15	11880	1.536209
011661	33.20	240	97.64	11980	1.712420
011661	38.18	260	90.88	11590	1.234648
011661	31.52	250	111.45	11840	3.899759
011761	31.52	240	67.71	11780	5.408849
011761	33.20	240	84.20	11950	4.759520
012361	31.52	270	101.85	11880	1.079536
012561	33.20	250	87.64	11940	1.400097
012561	37.23	250	98.61	11620	1.393563
012561	43.13	260	65.74	11370	1.194871
010462	31.52	250	81.69	11810	6.525340
010462	33.20	260	89.67	11980	2.172294
010562	33.20	240	80.63	11950	13.67418
010562	37.23	250	92.81	11620	1.686877
010562	38.18	260	105.37	11680	1.667577
011963	33.20	270	92.08	11730	1.115365
012163	33.20	260	103.35	11770	1.460469
012263	33.20	250	112.63	11750	2.122224
012363	33.20	250	110.70	11760	2.085791
013063	33.20	260	107.40	11720	1.655719

corresponding geopotential heights at 200 hPa are shown in the next column. The last column shows a computation of the ratio of the observed wind V and the gradient wind V_G. Here by gradient wind, we mean the normal (not anomalous) solution of the gradient wind equation.

In the last column, most entries have values greater than unity. Several of these values have magnitudes on the order of 5 or 6. Since these values were obtained directly from a straightforward calculation using the raw station data, it is apparent that the subtropical jet of Northern Hemisphere winter exhibits supergradient winds. Although only four years of data are considered here, this feature has been noted in all winter seasons.

For the definition of supergradient winds, another criterion can be considered. First, consider an alternative form of the gradient wind equation expressed by

$$V_G\left(\frac{\partial\beta}{\partial t}+f\right)=f\,V_g, \tag{5}$$

where $\partial\beta/\partial t$ is the relative angular velocity of an air parcel moving with speed V_G. Given also the

assumption that the parcel is in solid-body rotation at this angular velocity, the vertical component of the relative vorticity for the parcel would then be $\xi \equiv 2\partial\beta/\partial t$, so that

$$V_G\left(\frac{\xi}{2}+f\right)=f\,V_g, \tag{6}$$

or

$$\frac{\xi}{2}+f=\frac{2V_g}{V_G}. \tag{7}$$

From $V_G > 2V_g$, it can be shown that it is equivalent to say $-1 > \xi/f > -2$. Both of these methods were used by Mogil and Holle (1972) where a disagreement was found, specifically an area where the wind is such that $V_G = 2V_g$ did not match with $-1 > \xi/f > -2$, thus suggesting that solid-body rotation as an interpretation is incorrect.

3. Removal of supergradient winds by model initialization and data assimilation procedures

3.1 Normal-mode initialization

It was felt that overbalancing from the use of too many vertical modes within normal-mode initialization could be an important factor for the loss of anomalous supergradient winds. Kitade (1983) developed an algorithm for normal-mode initialization for the Florida State University (FSU) Global Spectral Model. Here the conventional adiabatic initialization has been extended to include diabatic effects [see also Daley (1981)]. This algorithm permits the inclusion of as many as five vertical modes. If more vertical modes are initialized, then the effect of this initialization is to balance the wind field with respect to the pressure field. If, however, only one or two modes are initialized then it is possible to retain some degree of unbalanced flow. Thus in principle, we believe that anomalous supergradient winds can be retained in the model's initialization if a smaller number of vertical modes are retained. In light of this belief, we have examined the resulting wind field obtained from various degrees of vertical mode initialization.

Usually, five vertical modes are used to remove high-frequency oscillations. When the initial state, which included supergradient winds, is subjected to normal-mode initialization, the supergradient winds may be rejected as illustrated in Fig. 3.

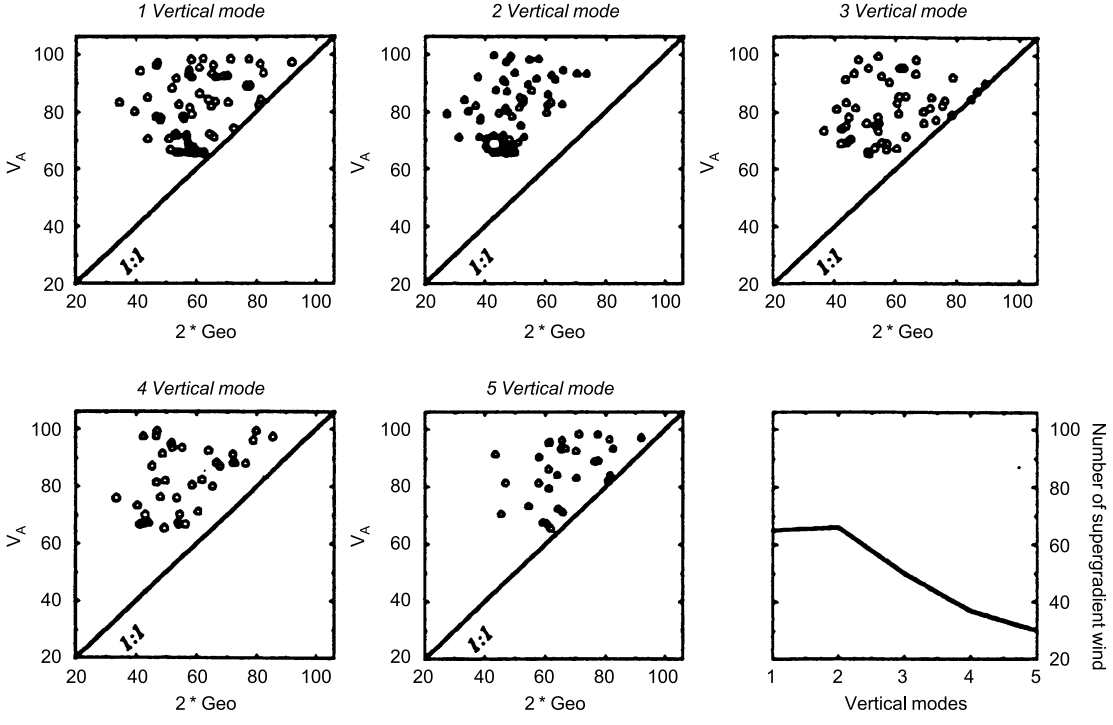

Fig. 3. Number of supergradient wind observations retained after normal-mode initialization as a function of the number of vertical modes

Consequently, normal-mode initialization is one of the procedures inherent to the model that can contaminate supergradient features and thus lead to large forecast errors. It is readily apparent in this illustration that a large number of supergradient winds are indeed retained when a smaller number of vertical modes are used. The reduction in the percentage of supergradient winds as a function of vertical modes is shown in the last panel. These results are based on five separate experiments. It is apparent that if we were either to exclude the normal mode initialization or to retain just one vertical mode (for balancing) then we can include 60% or more of the strong winds in the initial state. The other 40% may have been lost from the data assimilation constraints.

3.2 Multivariate optimum interpolation

A multivariate optimum interpolation code, acquired originally from the National Centers for Environmental Prediction (NCEP), has been applied to data sets of winds and temperature at several pressure levels. This code performs an analysis using the method proposed by Bergman (1978). We also follow this procedure to incorporate error characteristics; the error covariance matrix follows the rationale that the covariance function, $\overline{f_i \cdot f_j}$, is modeled by an analytical function to fit the observed forecast errors of geopotential heights. This analysis includes the evaluation of several auto-covariance functions between forecast and observations. This scheme, however, does include a geostrophic constraint. In requiring that the observations of the mass field be permitted to influence the analysis of the motion field, and vice versa, it became necessary to improve on the geostrophic constraint between the residuals of the mass motion field. As would be expected, the multivariate optimum interpolation procedure led to an immediate removal of the supergradient winds.

Based on the foregoing discussion, we conclude that in the operational forecasts of the 1980s the multivariate optimum interpolation contributed significantly to the removal of these strong winds in the initial state. We have since noted that the current 3D-Var and 4D-Var operational data assimilation schemes suffer from similar imposed constraints, thus degrading the initial wind analysis in anomalous wind situations. These constraints also may have broader consequences than described here, since these schemes will tend to remove any unbalanced flow in the initial state. Although this may be a desirable effect in general, it is evident that if the observed state is characterized by significant departures from either geostrophic or gradient wind balance, or even more generally from nonlinear (i.e., Charney) balance, the model initial conditions may be a poor representation of the observations. Further discussion of this issue is provided in the concluding section.

4. Results from global model experiments

Six 10 day forecasts were carried out with the T106 (Triangular Truncation, 106 waves) version of the FSU Global Spectral Model as described in the Appendix; three of these examples included supergradient winds and the other three did not. These forecasts were monitored by a standard skill score, specifically the anomaly correlation of the 500 hPa geopotential height. The procedure is described in the following sections.

4.1 Data sets

The global data sets used in this study came from the European Centre for Medium-Range Weather Forecasts (ECMWF) reanalysis data sets archived at the National Center for Atmospheric Research (NCAR). An inner domain over eastern Asia where supergradient winds are prevalent was specially reconsidered.

In this inner domain, raw upper-air data at 200 hPa and 300 hPa for 1200 UTC on 16 January 1979, 1 January 1980, and 18 January 1982 were obtained. The area from 15° S to 50° N, and from 95° E to 175° W defines this inner domain. Over this region, an objective analysis of the u and v components of the wind was carried out using the method of successive corrections with four scans through the data set. Figures 4–6 illustrate the ECMWF analysis; a difference between the ECMWF analysis and the objective analysis in the intensity of wind speeds on the order of $20\,\mathrm{m\,s^{-1}}$ was noted.

For the computation of supergradient wind we adapt a procedure based on Bell and Keyser

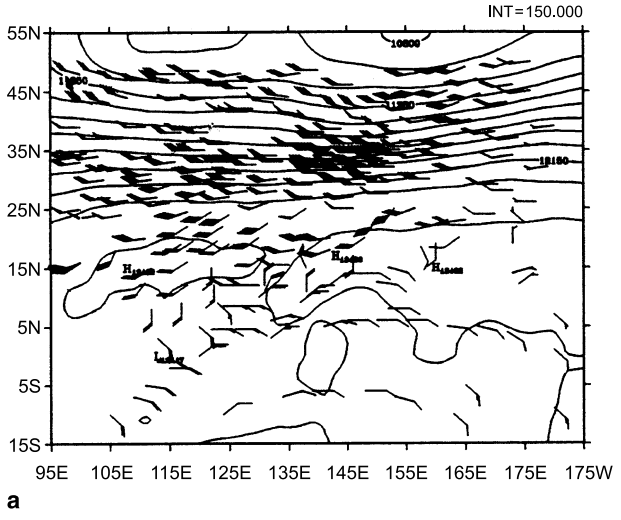

Fig. 4. Wind and geopotential height fields for (**a**) 200 hPa (top panel), and (**b**) 300 hPa (bottom panel), valid at 1200 UTC 16 January 1979

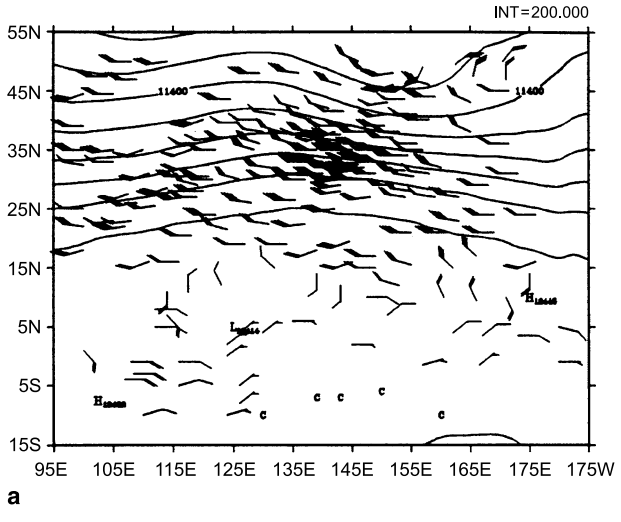

Fig. 5. Wind and geopotential height fields for (**a**) 200 hPa (top panel), and (**b**) 300 hPa (bottom panel), valid at 1200 UTC 1 January 1980

(1993). We rewrite the gradient wind equation (1) as

$$K_H V_G^2 + f V_G = b_n, \tag{8}$$

where V_G is the gradient wind, and $b_n = -g\partial z/\partial n$ measures the pressure gradient force normal to the flow. Thus, given b_n, we wish to map the streamlines and isotachs of the normal and the anomalous solution of the gradient wind equation, given respectively by

$$V_N = \frac{-f + (f^2 + 4b_n K_H)^{1/2}}{2K_H}, \tag{9}$$

and

$$V_A = \frac{-f - (f^2 + 4b_n K_H)^{1/2}}{2K_H}. \tag{10}$$

Here, the unknown quantities are b_n and K_H, defined respectively by

$$b_n = -g\frac{\partial z}{\partial n} = -g\left(\frac{u}{V}\frac{\partial z}{\partial y} - \frac{v}{V}\frac{\partial z}{\partial x}\right) \tag{11}$$

and

$$K_H = \frac{1}{V}\frac{d\alpha}{dt}, \tag{12}$$

where α is the angle defining the direction of the wind. Furthermore, following Bell and Keyser (1993), the rate of change of α is expressed as

$$\frac{d\alpha}{dt} = \frac{1}{V^2}(v\phi_x - u\phi_y) - f, \tag{13}$$

where

$$V = (u^2 + v^2)^{1/2}. \tag{14}$$

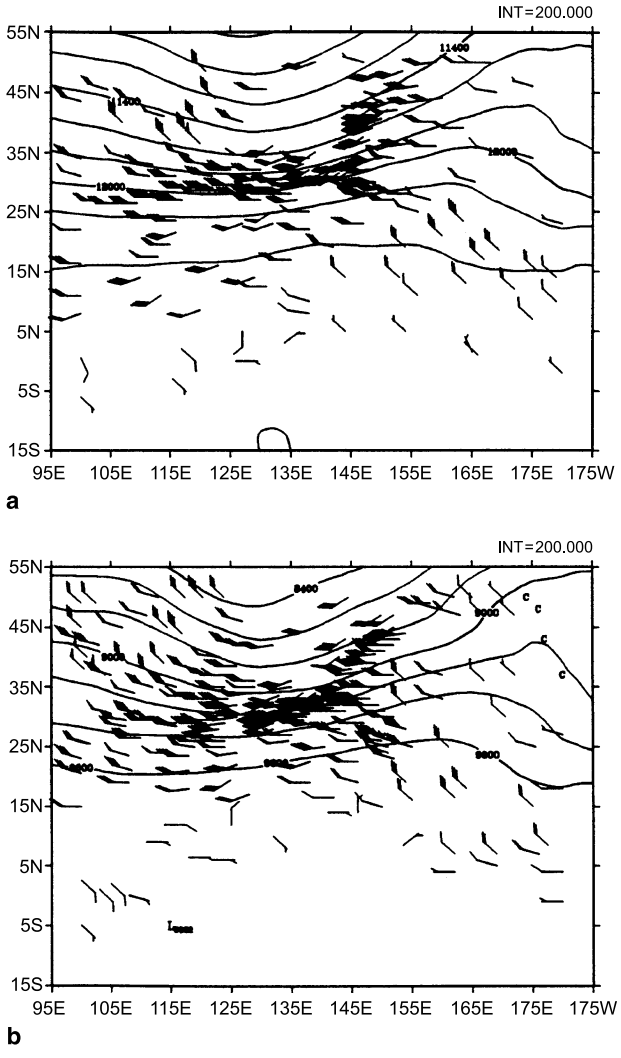

Fig. 6. Wind and geopotential height fields for (**a**) 200 hPa (top panel), and (**b**) 300 hPa (bottom panel), valid at 1200 UTC 18 January 1982

In Eq. (13),

$$\phi_x = g\frac{\partial z}{\partial x} \tag{15}$$

and

$$\phi_y = g\frac{\partial z}{\partial y} \tag{16}$$

are the geopotential gradients.

This computational scheme requires an iterative procedure starting with a first guess for u and v. Let u^n and v^n denote the n-th iteration of the wind components. The total wind V^n is determined from (14). The geopotential gradient b_n is determined from (11). The curvature K_H is determined from (12). Equations (9) and (10) determine the corresponding normal and anomalous wind speeds, V_N^n and V_A^n. The corresponding wind components, (u_N, v_N) and (u_A, v_A), are the starting point of the next iteration. This scheme converges within two or three iterations and describes a robust solution for the normal and the anomalous gradient winds. The geopotential height, z, is prescribed in this problem. A reverse algorithm has been developed for calculation of the wind direction at each grid point from the wind components. Using these wind directions and wind speeds, u and v at every grid point for anomalous gradient wind flow have been calculated at 200 hPa and 300 hPa, and are shown in Figs. 7–9 for each of the three times considered.

4.2 Improving the anomaly correlations

This section shows the forecast skills as measured by the anomaly correlation index. The definition of the anomaly correlation index is as follows:

$$\sigma = \frac{\left(\sum(x-\bar{x})\right)\left(\sum(y-\bar{y})\right)}{\left[\left(\sum(x-\bar{x})^2\right)\left(\sum(y-\bar{y})^2\right)\right]^{1/2}}, \tag{17}$$

where x is the difference at each grid point of the forecast and climatology, and y is the difference at each grid point of the observed and climatology. The sum is taken over both latitude and longitude.

Here we compare the results from two sets of experiments:

(i) *Control:* Here the operational analyses obtained from ECMWF are used for those cases in which significant forecast failures were noted. These sets of initial states failed to retain the strong observed anomalous winds south of Japan. The forecasts were made at a resolution of T106 and integrated out to 10 days; the initial states of the ECMWF analysis had been subjected to multivariate optimum interpolation for data assimilation and a multiple vertical-mode normal-mode initialization.

(ii) *Analyzed anomalous winds in the initial states:* Here we removed the ECMWF analysis over an inner domain covering the regions 95° E to 175° W and 15° S to 50° N. Over that region, the raw data for the winds and geopotential heights were reanalyzed using a simple successive correction scheme, following Cressman (1959), in order to

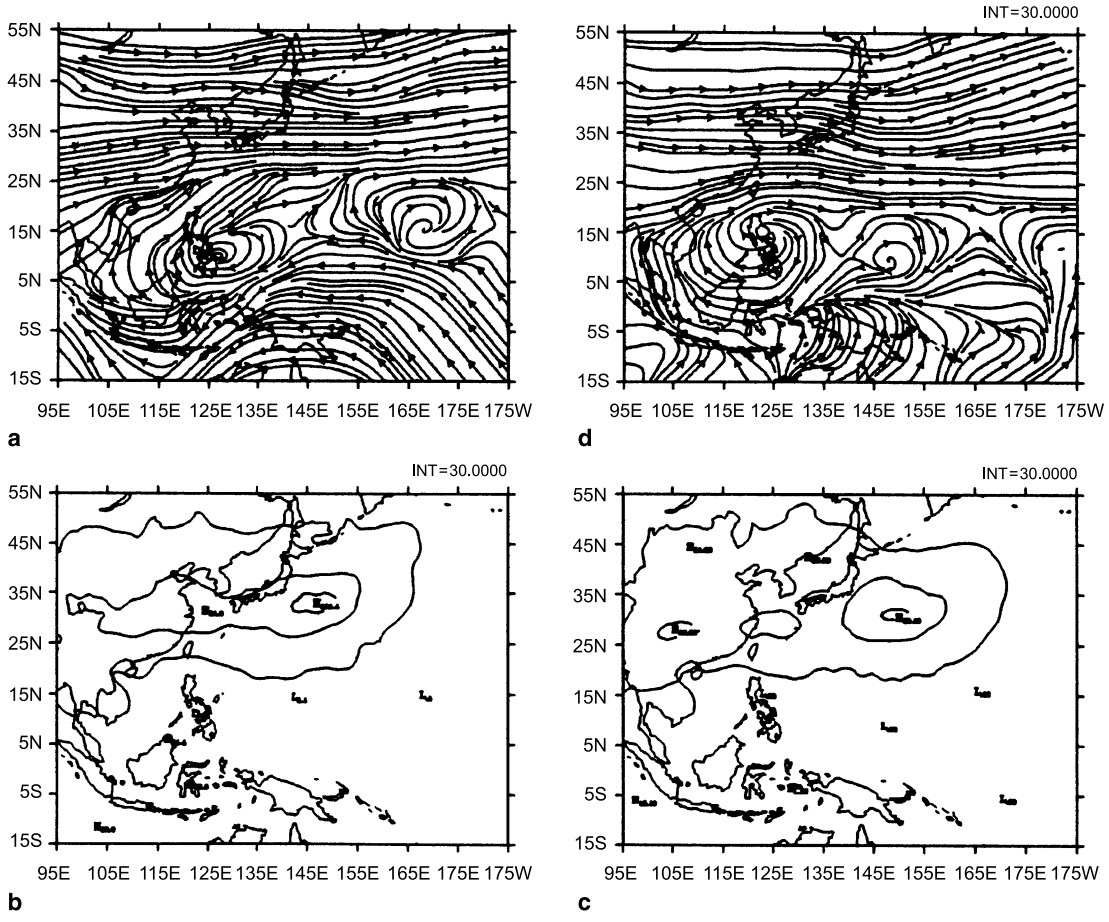

Fig. 7. Objectively analyzed streamlines (top panels) and isotachs (bottom panels) for 1200 UTC 16 January 1979. Left panels are for 200 hPa and the right panels are for 300 hPa

retain the anomalous winds. This inner and the outer ECMWF analysis were merged at the boundaries of the inner domain using a simple nine-point weighted smoothing. This simple procedure helped to retain these strong anomalous winds. It should be clarified here that the purpose of this procedure is definitely not to assert that a successive correction scheme needs to be brought back into analysis procedures. Rather, the aim is to demonstrate that it is necessary to find ways to retain these anomalously strong winds in order to overcome certain forecast failures.

Differences between the anomaly correlations for the two sets of experiments are summarized in Figs. 10–12. The inclusion of the anomalous winds does seem to have a strong positive impact on the 10-day global model forecasts. In Fig. 10a, the solid line shows the results of 500 hPa geopotential height field for the control experiments and the dashed line for the anomalous wind experiments over the globe. Figure 10b shows the same results for the 200 hPa level. The greatest impacts are seen between days 6 and 10 when the effects of the anomalous winds appear to have spread across the global domain. Figure 11 shows the corresponding results at 500 hPa over the inner regional domain, where the positive impact from the anomalous gradient winds was apparent from day 3 and was quite large. Also shown (Fig. 12) is the anomaly correlation of zonal wind at 200 hPa, averaged over the inner regional domain, clearly showing a significant positive impact after day 1 for the anomalous gradient wind experiments. Overall, it is apparent that a regional unbalanced flow appears to carry more information for improved forecasts.

One of the major features of these experiments was the negative PNA wave train emanating from the Asian coast eastwards across the Pacific

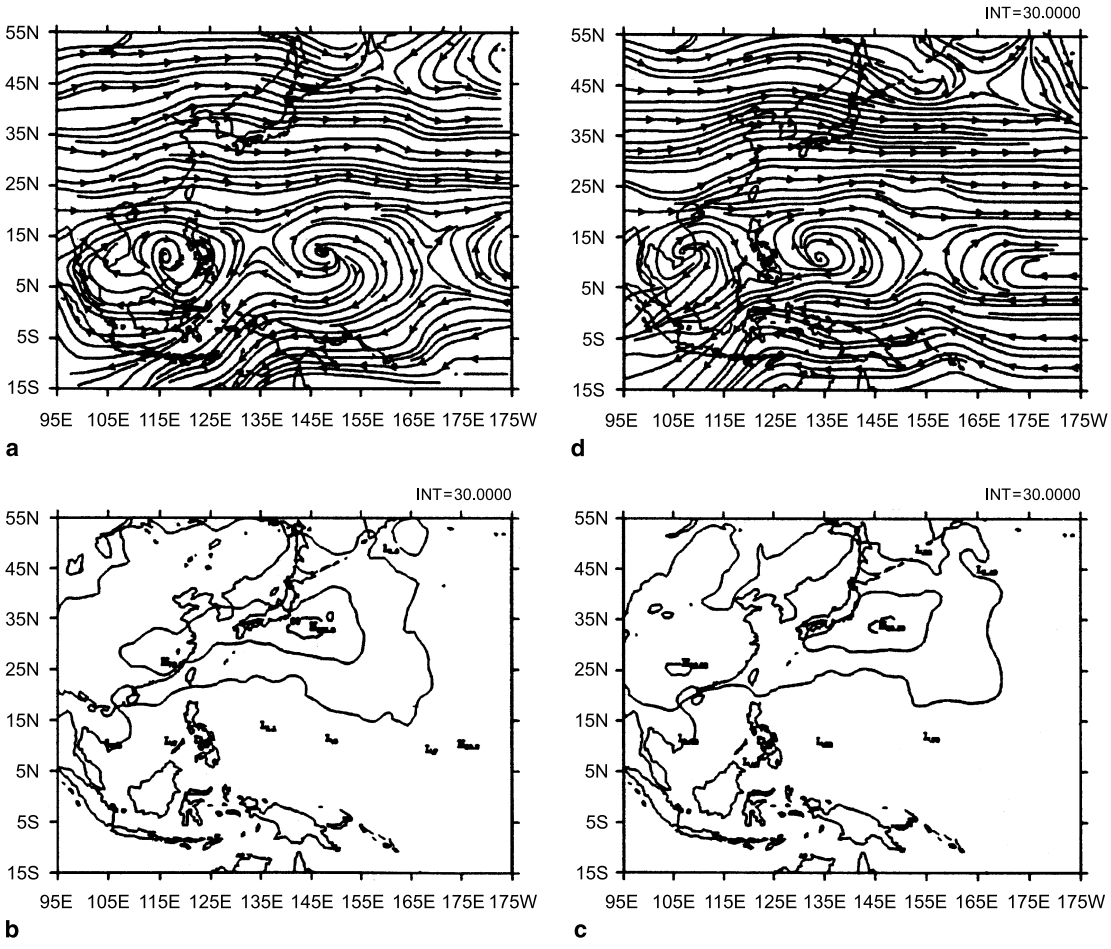

Fig. 8. Objectively analyzed streamlines (top panels) and isotachs (bottom panels) for 1200 UTC 1 January 1980. Left panels are for 200 hPa and the right panels are for 300 hPa

Ocean and over North America. It was noted that the overall improvements in the global anomaly correlation skill at 200 hPa after day 6 of forecasts appear to result primarily from the model's ability to predict this wave train, which was far better handled by the experiments that included the anomalous winds in the initial state.

5. Discussion and conclusions

In this paper, we have examined the presence and potential impacts of supergradient winds in the subtropical jet stream. These supergradient winds are frequently found in association with the negative phase of the PNA pattern in the Northern Hemisphere winter, and appear to be representative of the anomalous solution of the gradient wind equation. Such conditions were associated with some striking forecast failures in global forecast models of moderate resolution (e.g., Palmer, 1988). In this regard, it is noteworthy that these observed winds were not represented accurately in the initialized states of the then-current global models.

The primary conclusions of the present paper are as follows:

(i) The geostrophic constraints inherent to multivariate optimum interpolation schemes tend to degrade, or even remove, the supergradient winds.

(ii) The use of several vertical modes within normal-mode initialization schemes tends to overbalance the wind-pressure relationship, again degrading or removing the supergradient winds.

(iii) "Uninitialized" data sets that are not subjected to the above procedures within a global domain tend to carry more useful

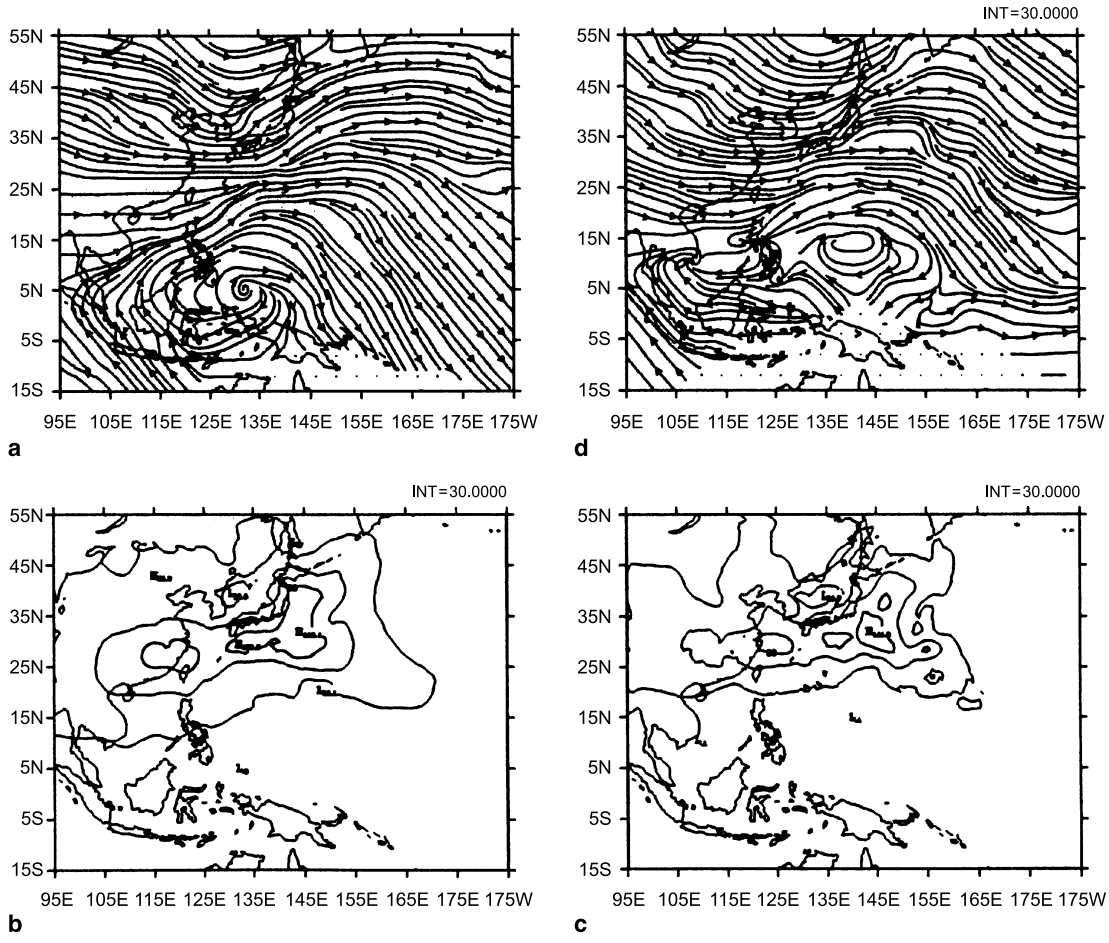

Fig. 9. Objectively analyzed streamlines (top panels) and isotachs (bottom panels) for 1200 UTC 18 January 1982. Left panels are for 200 hPa and the right panels are for 300 hPa

information on supergradient winds into the future.

(iv) The negative PNA wave train is predicted more accurately with the inclusion of these supergradient winds initially.

We have looked at recent data sets (raw data sets as well as assimilated fields) and noted that even the current 3D-Var and the 4D-Var data assimilation schemes carry geostrophic constraints and do not permit the presence of supergradient winds. This paper does not provide a future solution for this problem. Rather, we are stating that in these extreme wind situations, an analysis of the raw data using a simple successive correction provides insight into the nature of this forecast problem.

There are many practical issues related to the present study that were not addressed here. Based on our examination of observations, it is apparent that the lifetime of a supergradient wind episode appears to be on the order of three to four days. If a forecast is started prior to the initiation of such an episode, would the forecast model be able to capture this behavior? Since the gradient wind dynamics permit two solutions, how would a model recognize to go from one solution to the other on its own? It would be of considerable interest to examine the performance of models in the period leading up to a supergradient wind event to assess whether they are capable of capturing such an evolution, and to examine the associated implications for forecast skill. The converse problem is also one of great practical interest. Specifically, can a model select the correct solution of the gradient wind after the start of an experiment that includes anomalous gradient winds in the initial state but transitions towards normal gradient winds during the course

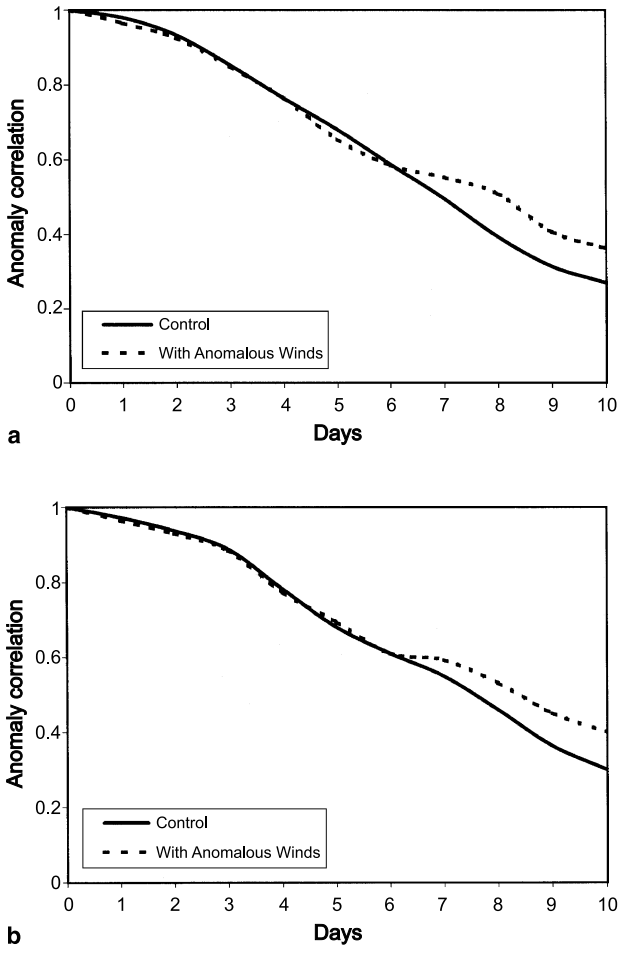

Fig. 10a. Anomaly correlation of the geopotential height field at 500 hPa over the globe from the control simulation (solid line) and from the simulation with anomalous winds (dashed line); (**b**) Anomaly correlation of geopotential height field at 200 hPa over the globe from the control simulation (solid line) and from the simulation with anomalous winds (dashed line)

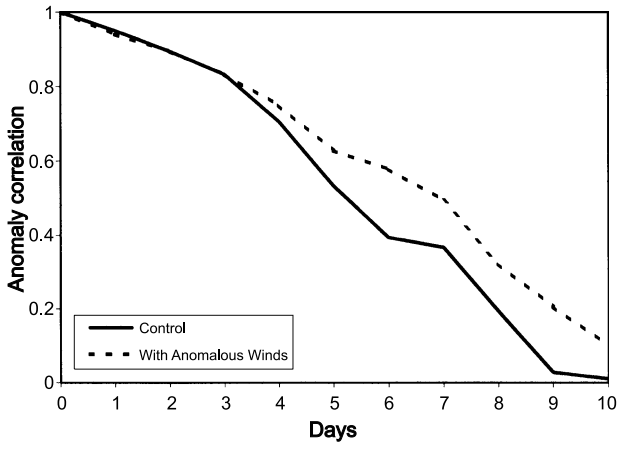

Fig. 11. Anomaly correlation of geopotential height field at 500 hPa over the inner regional domain (95° E–175° W; 15° S–50° N) from the control (solid line) and from the anomalous winds (dashed line) experiments

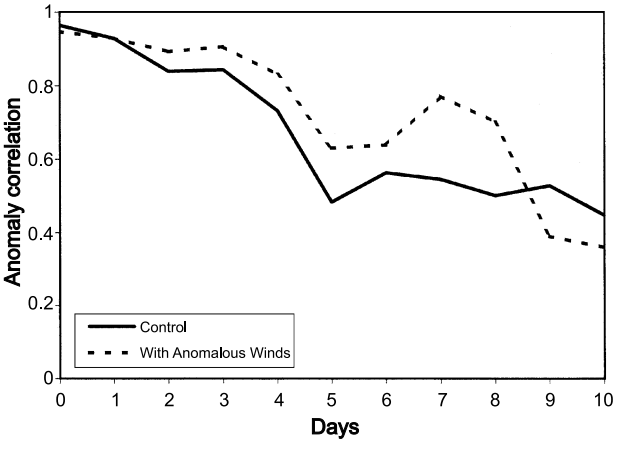

Fig. 12. Anomaly correlation of zonal wind at 200 hPa averaged over the inner regional domain (95° E–175° W; 15° S–50° N) from the control (solid line) and from the anomalous winds (dashed line) experiments

of the simulation? During a 10-day forecast we perceive the possibility of these states emerging more than once, and the question remains whether the models can accommodate such short (3- to 4-day) transitions.

A broader implication of the present results may be to the initialization problem. As noted above, current variational data assimilation schemes possess constraints that are based on the relationships of balanced dynamics (e.g., geostrophic balance; nonlinear balance). It is important to acknowledge that observed departures from such balances in the atmosphere may be associated with physically realistic (and thus highly significant) behavior, and not necessarily with measurement errors. A concrete example in this regard might be provided by the classical synoptic signature known to be conducive to the generation of inertia-gravity (i.e., unbalanced) waves in the troposphere: that is a mesoscale jet streak progressing from the trough to the downstream ridge of an amplifying wave in the jet stream (e.g., Uccellini and Koch, 1987; Koch and O'Handley, 1997). Typically in such cases, the associated flow not only is highly ageostrophic but also displays significant departures from nonlinear balance; it is unclear whether such flows, although observed, would be retained by a model's initialization scheme. Clearly, if the constraints built into these schemes remove these

departures from balanced flow, it is conceivable that the forecast will suffer, at least initially. This issue is likely to be equally important for high-resolution mesoscale models as it is for global models, if not more so. Nevertheless, how to design a general and effective procedure to "initialize" a model with a state that exhibits significant departures from any known balance relation is not immediately apparent, and represents an interesting direction for future research.

Appendix

The Florida State University (FSU) Global Spectral Model

The global model used in this study is identical in all respects to that used in Krishnamurti et al (1991). The T106 version of the model, however, has been highly vectorized to reduce the model integration time. In addition, moisture variable dew point depression ($T - T_d$) has been replaced by specific humidity and a look-up table is used for moisture calculation to further reduce the computational time. An outline of the model is as follows.

(1) Independent variables: λ, θ, σ, t.
(2) Dependent variables: vorticity, divergence, temperature and specific humidity. Horizontal resolution: triangular spectral truncation; T106 resolution has a 320×160 Gaussian transform grid with a horizontal separation of about 150 km at 20° latitude.
(3) Vertical resolution: 14 layers in the vertical between 50 hPa and 100 hPa. Model variables are staggered in the vertical using Charney-Phillips vertical discretization – vorticity, divergence, wind, and geopotential are located at the layer interface while temperatures, specific humidity and vertical velocity are assigned at the center of the layer. The vertical grid has higher resolution in the stratosphere and in the planetary boundary layer.
(4) Time integration scheme: The divergence equation, thermodynamic equation and pressure tendency equation are integrated implicitly while for the vorticity equation and the moisture continuity equation explicit time integration scheme is used. The tendencies of the physical processes are integrated using a forward time integration scheme.
(5) Space differing scheme: Spectral in the horizontal; centered differences in the vertical for all variables except moisture which is handled by an upstream differencing scheme.
(6) Surface topography is based on envelope orography (Wallace et al, 1983).
(7) Parameterization of physical processes:
   (a) Deep convection: based on modified Kuo cumulus parameterization scheme (Krishnamurti et al, 1983), where the moistening and mesoscale convergence parameters are obtained from 700 mb vorticity and mean vertical velocity averaged over cloud depth through a regression relation.
   (b) Shallow convection (Tiedke, 1984).
   (c) Dry convection.
   (d) Large-scale condensation (Kanamitsu, 1975). The scheme accounts for evaporation of falling precipitation.
   (e) Surface fluxes of heat, moisture and momentum are calculated using similarity theory (Businger et al, 1971).
   (f) Vertical distribution of fluxes in the free atmosphere is based on stability (Richardson number) dependent exchange coefficient (Louis, 1979).
   (g) 4th-order horizontal diffusion (Kanamitsu et al, 1983).
   (h) Long and shortwave radiative fluxes are based on band model and incorporate the radiative effects of water vapor, carbon dioxide, ozone and clouds (Harshvardan and Corsetti, 1989; Lacis and Hansen, 1974).
   (i) Parameterization of low, medium and high clouds for radiative transfer calculation is based on threshold relative humidity. Fraction area of various cloud distribution configurations in the vertical is based on random overlap consideration.
   (j) Surface temperatures: Prescribed over the oceans, while over the land a surface energy balance coupled to the similarity theory determines the surface temperature including its diurnal cycle (Krishnamurti et al, 1991).
(8) Nonlinear normal mode initialization: (Kitade, 1983), wherein the tendencies of first 5 modes with phase speed exceeding about 30 m s^{-1} are damped during the initialization. The slow moving higher modes are allowed to adjust freely.

Acknowledgements

This paper is based upon work originally undertaken by Mr. B. Annane. PC was supported by the National Science Foundation under Grant No. 0120333, awarded to the Florida State University.

References

Bell GD, Keyser D (1993) Shear and curvature vorticity and potential-vorticity interchanges: Interpretation and application to a cutoff cyclone event. Mon Wea Rev 121: 76–102

Bergman K (1978) Role of observational errors in optimum-interpolation analysis. Bull Amer Meteorol Soc 59: 1603–1611

Businger JA, Wyngaard JC, Izumi Y, Bradley EF (1971) Flux profile relationship in the atmospheric surface layer. J Atmos Sci 28: 181–189

Cressman G (1959) An operational objective analysis system. Mon Wea Rev 87: 367–374

Daley R (1981) Normal mode initialization. Rev Geophys Space Phys 19: 450–468

Harshvardan, Corsetti TG (1989) Long-wave parameterization for the UCLA/GLAS GCM. NASA Tech. Memo. 86072, Goddard Space Flight Center, Greenbelt, MD 20771, 52 pp

Holton JR (1992) An introduction to dynamic meteorology. New York: Academic Press, 511 pp

Kanamitsu M (1975) On numerical prediction over a global tropical belt. Report No. 75-1, Department of Meteorology, Florida State University, Tallahassee, FL, pp 1–282

Kanamitsu M, Tada K, Kudo K, Sato N, Isa S (1983) Description of the JMA operational spectral model. J Meteor Soc Japan 61: 812–828

Kitade T (1983) Nonlinear normal mode initialization with physics. Mon Wea Rev 111: 2194–2213

Koch SE, O'Handley C (1997) Operational forecasting and detection of mesoscale gravity waves. Wea Forecast 12: 252–281

Krishnamurti TN, Low-Nam S, Pasch R (1983) Cumulus parameterization and rainfall rates II. Mon Wea Rev 111: 816–828

Krishnamurti TN, Xue J, Bedi HS, Ingles K, Oosterhof D (1991) Physical initialization for numerical weather prediction over the tropics. Tellus 43AB: 53–81

Lacis AA, Hansen JE (1974) A parameterization of the absorption of solar radiation in the Earth's atmosphere. J Atmos Sci 31: 118–133

Louis JF (1979) A parametric model of vertical eddy fluxes in the atmosphere. Bound Layer Meteorol 17: 187–202

Mogil M, Holle RL (1972) Anomalous gradient winds: Existences and implications. Mon Wea Rev 100: 709–716

Newton CW (1959) Axial velocity streaks in the jet stream: Ageostrophic inertial oscillations. J Meteorol 16: 638–645

Palmer TN (1988) Medium and extended range predictability and stability of the PNA mode. QJR Meteorol Soc 114: 691–713

Tiedke M (1984) The sensitivity of the time-mean large-scale flow to cumulus convection in the ECMWF model. Workshop on convection in large-scale numerical models, ECMWF, November 1983, pp 297–316

Uccellini LW, Koch SE (1987) The synoptic setting and possible energy sources for mesoscale wave disturbances. Mon Wea Rev 115: 721–729

Wallace JM, Gutzler D (1981) Teleconnections in the geopotential height field during the Northern Hemisphere winter. Mon Wea Rev 109: 784–811

Wallace JM, Tibaldi S, Simmons AJ (1983) Reduction of systematic forecast errors in the ECMWF model through the introduction of envelope orography. QJR Meteorol Soc 109: 683–718

Corresponding author's address: Dr. Philip Cunningham, Department of Meteorology, The Florida State University, Tallahassee, Florida 32306-4520, USA (E-mail: cunningham@met.fsu.edu)

Verleger: Springer-Verlag GmbH, Sachsenplatz 4–6, 1201 Wien, Austria. – Herausgeber: Prof. Dr. Reinhold Steinacker, Institut für Meteorologie und Geophysik, Universität Wien, Althanstraße 14, 1090 Wien, Austria. – Redaktion: Althanstraße 14, 1090 Wien, Austria. – Satz und Umbruch: Thomson Press (India) Ltd., Chennai. – Druck und Bindung: Grasl Druck&Neue Medien, 2540 Bad Vöslau, Austria. – Verlagsort: Wien. – Herstellungsort: Bad Vöslau. – Printed in Austria.